# Numerical Simulation of Wind-Aided Turbulent Fires in a Ventilated Model Tunnel

H. Y. WANG and P. JOULAIN
Laboratoire de Combustion et de Détonique
C.N.R.S. UPR 9028 -E.N.S.M.A., Université de Poitiers
BP 109 - Site du Futuroscope
86960, Futuroscope Cedex, France

## ABSTRACT

Numerical study is performed to investigate an intermediate scale, turbulent fires in a horizontal model tunnel exposed to air flow ranging from 0.5 to 2.5 m/s. Controlling mechanisms of three dimensional flow, combustion, soot production and radiation are coupled with a Large Eddy Simulation. The computed, time-averaged flame length and height are compared with experimental data, and a relatively good agreement is attained. It is found that the persistent flame length is approximately 3-4 times the pyrolysis length, and however, the intermittent flame length is up to 6 times the pyrolysis one. The minimum air velocity of 1 m/s is predicted to suppress the hotter backlayering flow upstream of the fire section in a tunnel. As the air velocity decreases, radiation increasingly becomes the dominant mode of heat transfer from the flame to the wall surface.

**KEY WORDS :** Large-Eddy-Simulation, turbulent fires, backlayering flow, ventilated tunnel

## INTRODUCTION

Many studies have been conducted with the motivation of improving our understanding on the effects of fires in tunnels. An analytical relation [1] for determining the critical velocity required to suppress the backlayering flow upstream of the fire section is available. The values of the flame height/length have been obtained mainly from sets of equations derived by applying Froude number preservation, combined with some experimental data [2, 3]. The smoke movement is experimentally studied [4, 5, 6] by using a horizontal model tunnel with propane gas burners as fire sources. The buoyancy effects in turbulent reacting flow have been the subject of many investigations [7, 8] by advanced numerical techniques. It was found [7, 8] that the buoyancy-related modifications in the standard $k-\varepsilon$ turbulence model strongly affected the extent of upstream propagation of the backlayering against the ventilation. So far, the analytical relation can't describe correctly the experimental flame shape (height/length) in a ventilated tunnel due to the carelessness of the buoyancy effects. Moreover, it seems still lack of a complete and detailed examination about how a wind-aided turbulent fire is evolved spatially and temporally inside the tunnel.

This article presents an application of Large-Eddy-Simulation (LES) for solving the fluid dynamic equations of three-dimensional elliptic, reacting flow. In this work, the fire itself is prescribed in a manner consistent with mixing-controlled combustion. The NIST fire code [9] based on a mixture-fraction combustion model is used. While the combustion and soot models both based on an Eddy-Break-Up (EBU) approach [10] have been added by the present authors. The two combustion models are tested for the wind-aided turbulent fires. The large scale transport of combustion products can be simulated directly, but combustion processes occuring at small length and time scales are represented in an approximate manner. This approach to the field modeling of fire phenomena emphasizes high enough spatial and temporal resolution with an efficient flow solving technique, developped by McGrattan [9]. The main advance lies in the modeling of burnout behind the pyrolysis region, and identification of the time-dependent persistent flame, intermittent flame and buoyant plume. A three-dimensional, transient field model predictions are presented, and the time-averaged flame height/length, and flame-surface heat flux are compared with the experimental data [5, 6].

**THEORETICAL ANALYSIS**

The starting point of the analysis is the set of three-dimensional, partial differential equations that governs the phenomena of interest here. This set consists, in general, of the following equations : the continuity equation, the three momentum equations that govern the conservation of momentum per unit mass in each of the three space dimensions, the equation for conservation of mixture fraction, and the radiative transfer equation. The key features of each of these will be briefly described.

**Flowfield Model**

LES is based on a filtering operation, which decomposes a full flowfield, $\phi(x,t)$, into a resolved component $\overline{\phi}(x,t)$ and a SubGrid-Scale (SGS) component $\phi'(x,t)$ [11]. The resolvable-scale component, $\overline{\phi}(x,t)$, is obtained from its full field, $\phi(x,t)$, by employing a filter $G(x,\Delta)$ of specified width $\Delta$ :

$$\overline{\phi}(x,t) = \int_{\Omega} G(x-x',\Delta)\phi(x',t)dx' \tag{1}$$

where $\Omega$ is the domain of interest. Applying the filtering operation to each term in the conservation equations of mass, momentum, energy and species, and decomposing the dependent variables (u, v, w, p, etc) into resolved and subgrid components results in the filtered governing equations, shown below :

$$\frac{\partial \rho}{\partial t} + \frac{\partial \rho\,\overline{u}_j}{\partial x_j} = 0 \tag{2}$$

$$\frac{\partial \rho\,\overline{u}_i}{\partial t} + \frac{\partial (\rho\,\overline{u}_i\,\overline{u}_j)}{\partial x_j} + \frac{\partial \overline{p}}{\partial x_i} - \rho\,g_i = \nabla(\overline{\tau}_{ij} + \overline{\tau}_{ij,SGS}) \tag{3}$$

where an overbar denotes the filtered variable. The unresolved field, $\phi'(x,t)$, given as

$$\phi'(x,t) = \phi(x,t) - \overline{\phi}(x,t) \qquad (4)$$

is modeled by the Smagorinsky model [11]. In this model, the SGS Reynolds stresses tensor, $\overline{\tau}_{ij,SGS}$, are related to the local large scale rate of strain.

$$\overline{\tau}_{ij,SGS} = 2\mu_t \overline{S}_{ij} \qquad (5)$$

where $\overline{S}_{ij} = \dfrac{1}{2}\left(\dfrac{\partial \overline{u}_i}{\partial x_j} + \dfrac{\partial \overline{u}_j}{\partial x_i}\right)$ and $\mu_t = C_s^2 \rho \Delta^2 \left|\overline{S}_{ij}\right|$ $\qquad (6)$

Here, $\left|\overline{S}_{ij}\right|$ is the magnitude of the large scale strain rate tensor $\overline{S}_{ij}$, and $\Delta$ the filter width. In the calculations, the length scale of eddy viscosity is tied to the grid as $\Delta = (\Delta x \Delta y \Delta z)^{1/3}$, and its time scale is determined by the local resolvable dissipation. In this study, the standard value of $C_s$=0.2 is assigned, because modifications of the Smagorinsky constant don't give acceptable agreement in a wide range of wind-aided fire conditions. It should be pointed that the SGS correlations for turbulent enthalpy flux are extremely difficult to model accurately. Thus, most SGS models are based on an eddy viscosity assumption, resulting in the following energy equation :

$$\frac{\partial \rho \overline{h}}{\partial t} + \frac{\partial(\rho \overline{u}_i \overline{h})}{\partial x_j} - \frac{D\overline{p}}{Dt} = \frac{\partial}{\partial x_j}\left(\frac{\mu_t}{Pr_t}\frac{\partial \overline{h}}{\partial x_j}\right) + \dot{q}_c + q_r \qquad (7)$$

where $Pr_t$ denotes the turbulent Prandtl number ($Pr_t$=0.7), $\dot{q}_c$ the rate of heat release per unit volume, and $q_r$ the radiant energy flux. Finally, the perfect gas law is used to describe the equation of state.

**Combustion Model**

Two combustion models based on an eddy-viscosity approach are briefly described here. It is assumed that combustion of a hydrocarbon fuel is mixing controlled, and chemical reaction proceeds through the single irreversible step,

$$4C_nH_m + (4n+m)O_2 \rightarrow 4nCO_2 + 2mH_2O \qquad (8)$$

The first combustion model is described by a mixture fraction equation, written as,

$$\frac{\partial \rho \overline{f}}{\partial t} + \frac{\partial(\rho \overline{u}_j \overline{f})}{\partial x_j} = \frac{\partial}{\partial x_j}\left(\frac{\mu_t}{Sc_t}\frac{\partial \overline{f}}{\partial x_j}\right) \qquad (9)$$

where $Sc_t$ denotes the turbulent Schmidt number ($Sc_t$=1). The oxygen mass conservation equation can be transformed into an expression for the local reaction rate, which is calculated through Eq. 9 for $\partial \overline{f}/\partial x_j$ and a state relation [9] for $dY_o/df$

$$-\dot{\omega}_o = \frac{\partial}{\partial x_j}\left(\frac{\mu_t}{Sc_t}\frac{dY_o}{df}\frac{\partial \overline{f}}{\partial x_j}\right) - \frac{dY_o}{df}\frac{\partial}{\partial x_j}\left(\frac{\mu_t}{Sc_t}\frac{\partial \overline{f}}{\partial x_j}\right) \qquad (10)$$

According to Huggett [12], the heat release rate is directly proportional to the rate of consumption of oxygen, $\dot{q}_c = H_o \dot{\omega}_o$. Here $H_o$ is the heat release rate per unit mass of oxygen consumed.

In the second model, the combustion processes are governed by the conservation equation for the filtered mass fraction of fuel gases ($\overline{Y}_f$) and oxydan ($\overline{Y}_o$), written as,

$$\frac{\partial \rho \overline{Y}_n}{\partial t} + \frac{\partial (\rho \overline{u}_j \overline{Y}_n)}{\partial x_j} = \frac{\partial}{\partial x_j}\left(\frac{\mu_t}{Sc_t}\frac{\partial \overline{Y}_n}{\partial x_j}\right) - \dot{\omega}_n \qquad \text{(n=f and o)} \qquad (11)$$

The gas-phase oxidation reaction is characterized by an Eddy-Break-Up model [10],

$$\dot{\omega}_f = \rho\, C_R \frac{\varepsilon}{k} \min(\overline{Y}_f , \frac{\overline{Y}_o}{\upsilon_f}) \qquad (12)$$

Here $\nu_f$ is mass stoichiometric oxidant/fuel ratio. The Eddy-Break-Up constant, $C_R$, is modeled with a viscous mixing model as,

$$C_R = 23.6\left(\frac{\mu\varepsilon}{\rho k^2}\right)^{1/4} \qquad (13)$$

The turbulent kinetic energy is expressed as,

$$k = \left(\frac{\mu_t}{C_\mu \rho \Delta}\right)^2 \qquad (14)$$

The relation for the dissipation of turbulent kinetic energy is,

$$\varepsilon = C_\varepsilon \frac{k^{3/2}}{\Delta} \qquad (15)$$

Here the constants $C_\mu$ and $C_\varepsilon$ are given as 0.0856 and 0.845, respectively. The heat release rate is directly proportional to the rate of consumption of fuel, $\dot{q}_c = H_f\,\dot{\omega}_f$. Here, $H_f$ is the heat release rate per unit mass of fuel consumed.

**Soot Formation and Combustion**

The two-equations soot model is used to predict soot concentration ($c_s$). The soot formation and its combustion are incorporated into a turbulent flow calculation in two convection-diffusion equations that compute a presursor particle number density and soot concentration. The interaction between soot combustion and turbulence is modeled according to the Eddy-Break-Up concept [10] formulated as,

$$R_{comb} = C_R \rho\, c_s \frac{\varepsilon}{k} \min\left(1, \frac{\overline{Y}_o}{c_s \nu_s + \rho \overline{Y}_f \nu_f}\right) \qquad (16)$$

**Radiation Model**

The radiation intensity, I, is found by solving the Radiative Transfer Equation (RTE) without scattering,

$$\vec{\nabla}.\vec{\Omega}I + \kappa I = \kappa \frac{\sigma \overline{T}^4}{\pi} \qquad (17)$$

This equation is solved through the use of a Finite Volume Method [9]. For EBU model, overall absorption coefficient for the soot and gas mixture is calculated through Modak model [13] in function of the temperature and concentration of combustion products. The soot volume fraction ($f_v$) is obtained at any location from the two-equations soot model. The radiative source term, $q_r$, in Eq. 7 is calculated from the divergence of the radiative flux, given as

$$q_r = -\int_{4\pi} \vec{\nabla}.\vec{\Omega}\, I.d\Omega \approx \kappa(\sum_{l=1}^{L} w^l I^l - 4\sigma \overline{T}^4) \tag{18}$$

**Method of Resolution**

The finite-difference technique is used to discretize the partial differential equations. This procedure entails the subdividing of the calculation domain into a finite number of cells. The velocities ($u_i$) are taken on the boundary of each cell; and all the scalar variables are taken at cell centers. This staggered grid leads to a very efficient differencing scheme for the equations. All spatial derivatives are approximated by second-order central differences and the flow variables are updated in time using an explicit second-order Runge-Kutta scheme. The pressure is found by taking the divergence of the momentum equations, yielding a Poisson equation which is solved with a direct solver [9]. The inert solid surface is considered as adiabatic, and the no-slip condition is imposed by setting all velocities to zero. The burning surface is considered as a pure combustible material ($\overline{f}_s = 1$ or $\overline{Y}_{f,s} = 1$).

**RESULTS AND DISCUSSION**

The schematic diagram of the release examined experimentally, and the coordinate system adapted in numerical simulation are shown in Figure 1. The analytical procedure used in
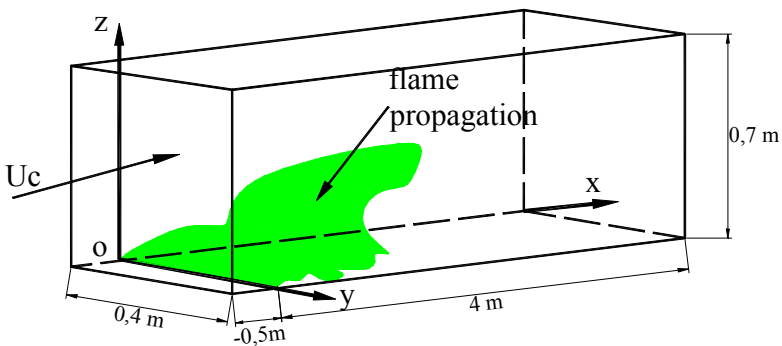


Fig. 1 - Wind-aided fire, and the coordinate system for numerical simulation

experiment is described in detail in Ref. [5] and briefly discussed here. The tests used sintered bronze burner which was mounted on a horizontal plate with a length of 4.5 m and a width of 0.4 m. Propane as fuel is uniformly injected through the burner surface with a width of 0.4 m and a length ($x_b$) of 0.25 m. The fuel injection rate is 0.01 kg/m²s, adjusted to give theoretical heat releases of 45 kW. In the x direction, start at 2 cm in the combustion zone, and stretch to about 6 cm at the free boundary. In the z direction, cell sizes are about 0.5 cm near the burning wall and stretch to about 6 cm far away from that region. Uniform grid is used in the half of the channel. No significant difference of the predicted results with different grid systems is observed. It was found that the mildly stretched grid system, 160 (x) x 10 (y) x 36 (z), offered the best tradeoff between accuracy and cost. The model is run in transient mode with about 8600 time steps. Using a DEC workstation, CPU times were of the order of 6 h for a real 30 s simulation by using the mixture fraction combustion model. While the CPU times increase by about 30% with the EBU model.

Although the wind-aided fires behind a pyrolysis region display a 3D behavior, only the time-averaged flame length and height on the median plane (x-z, y=0.2 m) are chosen for comparison between experiment and prediction. A maping flame luminosity technique [5, 6] using a CCD camera was developed to measure the visible flame height through images processing using a selected luminosity threshold. The buoyant instability may introduce strong perturbations during experiment, yielding the measured values with an uncertainty of 10-15%. It was checked that the so-determined persistent flame regime corresponds to a gas temperature of about 500 °C. The flame temperature in the intermittent regime is between 250 and 500 °C, and the buoyant smoke has temperature less than 250 °C. This criterion is also used for determining the predicted mean flame shape obtained through the time-averages of the instantaneous temperature output over a range of the computational time. The differences in the mean flame structure by using EBU and mixture fraction combustion models are clearly shown in Figures 2-3. The predicted time-averaged flame height/length with EBU and mixture fraction models, are compared with the experimentally-determined ones in Figure 4 as function of the wind velocity. According to experiment, the flame length progressively increases with wind velocity. For low wind velocity ($U_c \leq 1$ m/s), the flame length is correctly predicted by using EBU model as compared to the experimental data, and however, overpredicted about 40% by using mixture fraction model. In contrast, for high wind velocity ($U_c \geq 1.5$ m/s), the prediction of the flame length by using mixture fraction model is much improved, and however, worse
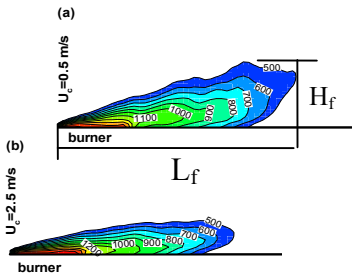


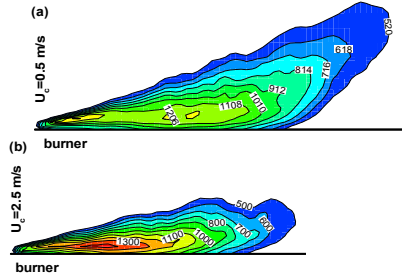Fig. 2 - Predicted persistent flame model



Fig.3 – Predicted persistent flameshape with EBU shape with mixture-fraction model

by using EBU model with an underprediction of about 30%. Agreement between predicted and measured flame height is relatively good by using EBU model in a range of wind velocity from 0.5 to 2.5 m/s, and worse by using mixture-fraction model with an overprediction of 10-50%. Globally, the predicted flame shape by using EBU model closely follows the general behavior of the experimental flame. Thus only the predicted results by using EBU model will be presented in the following sections.
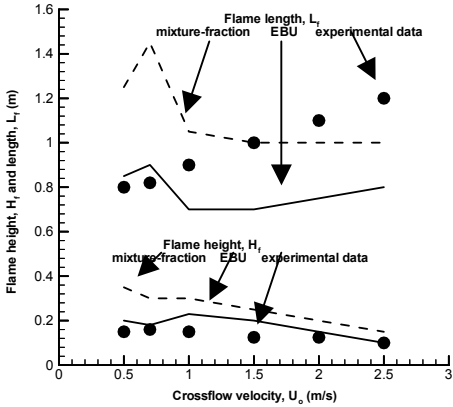


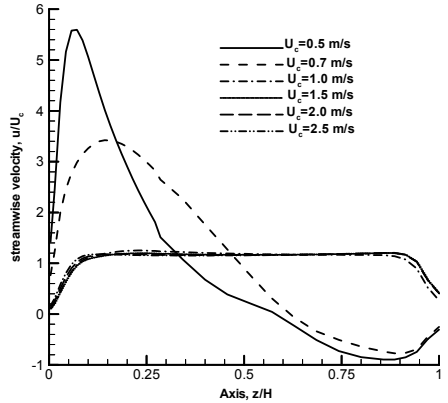Fig. 4 - Predicted (lines) and experimentally-determined (symbols) flame height and length

Fig. 5 - Predicted profiles of the mean axial velocity upstream of the burner (x=-0.2 m)

One of the practical interests of the wind-aided fire simulation is the prediction of critical velocity required to suppress the backlayering flow upstream of the fire section in tunnel. The predicted profiles of the mean axial velocity normalized by the inlet velocity, $U_c$, upstream of the burner (x=-0.2 m) as a function of the wind velocity are plotted in Figure 5. Following the Lavid analysis [1], the parameter, $\zeta = Gr_x / Re_x^{5/2}$ allows to characterize the turbulent flow regimes if the flame temperature is chosen as $T_f$=1150 K for estimating the local Grashof number.

- For the wind velocity lower than 1 m/s, the value of $\zeta$ is close to 1, the magnitude of the buoyancy and inertia forces is almost identical. The backlayering flow upstream of the fire section occurs, characterized by the negative velocity value as shown in Figure 5. The fire acts as a thermal blockage, this results in an acceleration of the air stream as it approachs the fire due to the combined effects of natural convection and air entrainment. The air flow velocity is increased by about 5 times for $U_c$=0.5 m/s, and 3 times for $U_c$=0.7 m/s from the original magnitude. The extent of the backlayering flow decrease as wind velocity increases from 0.5 to 0.7 m/s.

- For the wind velocity higher than 1 m/s, the value of $\zeta$ becomes much smaller than 1, the flow is dominated by the inertia force, and backlayering flow does not occur. The predicted profiles of the axial velocity are very similar due to turbulence development with a positive value in the cross-section, as shown in Figure 5.

The time-averaged temperature contours upstream and downstream of the fire section as a function of the wind velocity on the median plane (x-z, y=0.2 m) are presented in

167

Figure 6. The shaded areas denote the persistent flame shape. In the downstream direction, a rapid decrease in temperature peak is observed as energy is convected and conducted away from the hot flame region. A wind-aided fire plume in channel consists of three distinct regimes.

- As the wind velocity is lower than 1 m/s ($\zeta \approx 1$), the buoyant smoke flow impinges on the tunnel ceiling, and there is a persistent hotter (about 200-300 °C) backlayering flow upstream of the fire section.
- As the wind velocity is between 1 and 1.5 m/s, the buoyant smoke flow with about 100 °C reaches the ceiling, and occupies the upper part of the tunnel downstream of the fire section.
- As the wind velocity is higher than 2 m/s ($\zeta \ll 1$), the buoyant smoke flow disappears upstream and downstream of the fire section.
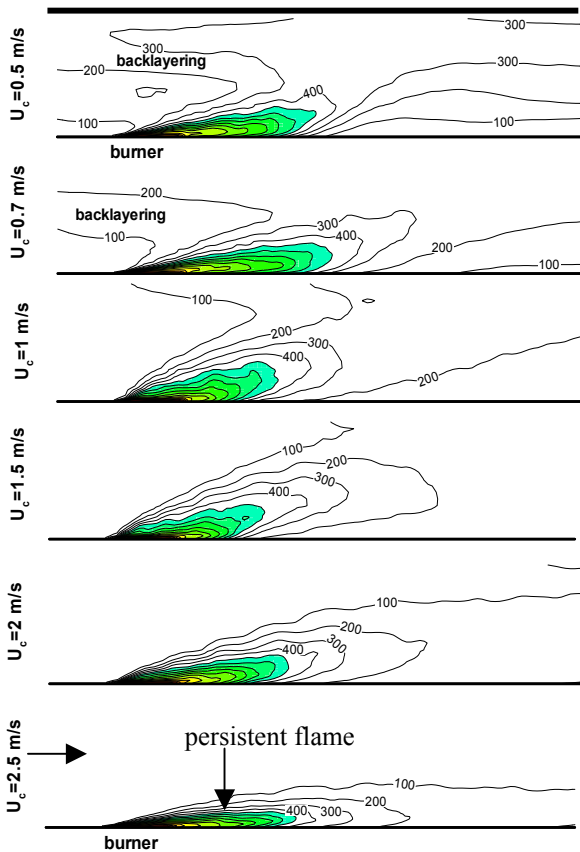


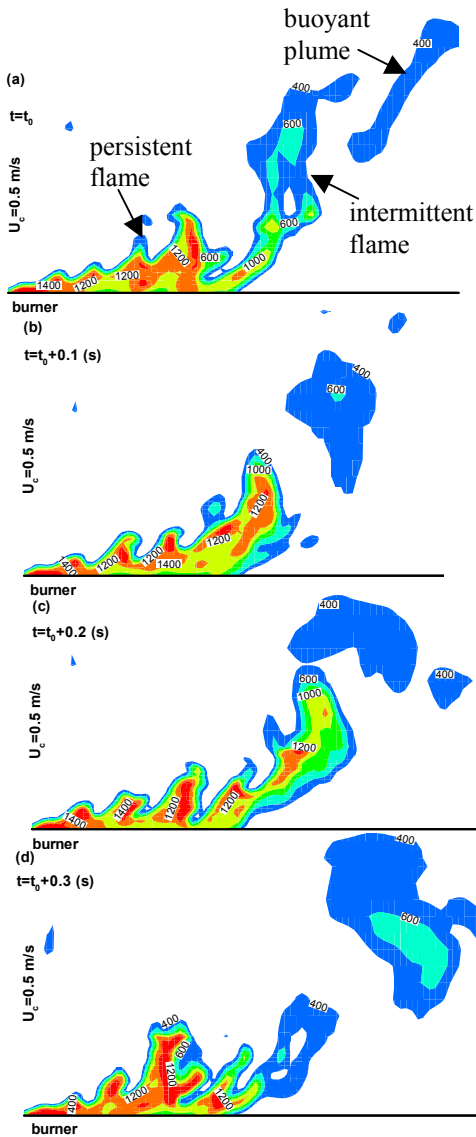Fig. 6 - Time-averaged temperature contours as a function of the wind velocity

Fig. 7 - Predicted instantaneous flame shapes
flame at $U_c$=0.5 m/s
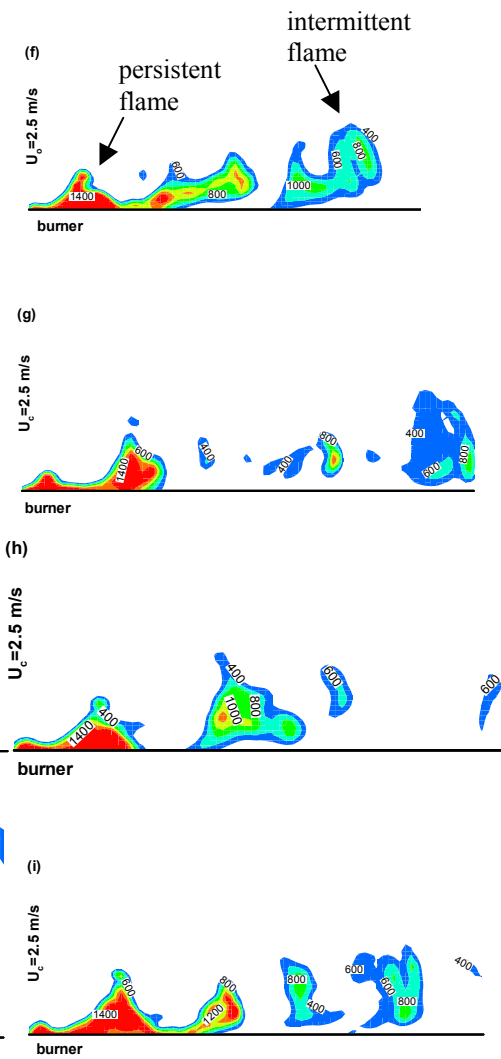
Fig. 8 - Predicted instantaneous
shapes at $U_c$=2.5 m/s

The simulated instantaneous fire plumes on the median plane (x-z, y=0.2 m) for two wind velocities of 0.5 and 2.5 m/s in a time interval of 0.1 s are shown in Figures 7-8. The flame structure traces vary significantly with time, indicating non-steady behaviour of the wind-aided fire propagation. For the low wind velocity ($U_c$=0.5 m/s), three distinct regimes, such as persistent flame, intermittent flame and buoyancy smoke are predicted as shown in Figure 7. The fire plume is first elongated in the downstream direction, and later tilted at a certain angle from the horizontal. The buoyant smoke is detached to the intermittent flame, reaching the ceiling. Several roll-up vortex structures are developed

along the boundary surface of the persistent flame. The strength of the vortex structure motions causes distortions of the temperature distribution, and in turn produces a vertical and horizontal oscillation of the persistent flame. The movement of the buoyant smoke flow is rather random due to the turbulent behavior, producing a complex highly oscillated temperature field. Buoyancy effect in a weakly ventilated tunnel produces oscillatory behaviour in flame structure in cyclic fashion as shown in Figure 7(a-d), consistent with the exprimental observations [5, 6]. This behaviour could manifest itself as the puffs of the intermittent flame and buoyant plume. However, as the wind velocity is increased to 2.5 m/s, both the persistent and intermittent flames are elongated in the downstream direction, and buoyant smoke is not predicted. In this case, the turbulent dissipation rate becomes strong, resulting in quenching of the diffusion flame characterized by the local flame extinction in the intermittent flame region. The numerical results suggest that the frequency of flame oscillation varies with the wind velocity. However, at this stage it is unclear if the behaviour noted here is a physical or numerical manifestation for identifying the frequency due to the numerical noise as the grid resolution is insufficient (2-3 cm). Moreover, it should be noted that the extent of instantaneous high temperature region (T>400 °C) is about 6 times the pyrolysis length. However, the time-averages of the output of this kind (Figures 7-8) of simulation generate a stable diffusion flame with a flame length of 3-4 times of the pyrolysis length as shown in Figures 2-3.

The predicted soot volume fraction contours for two wind velocities of 0.5 and 2.5 m/s are presented in Figure 9. As the wind velocity is lower than 1 m/s, the formed soot during combustion is transported up to ceiling by the buoyant plume through convection, as illustrated in Figure 9(a). However, for the strong wind velocity ($U_c$=2.5 m/s), boundary layer diffusion plays a dominant role on soot distribution, as shown in Figure 9(b). In all the cases, soot production seems to occur close to the high temperature fuel-rich zone, and decays rapidly once in the fuel-lean (core flow) region. A peak soot volume fraction value of about $1 \times 10^{-6}$ is predicted to occur near the burning surface, and this peak value is insensitive to the wind velocity.
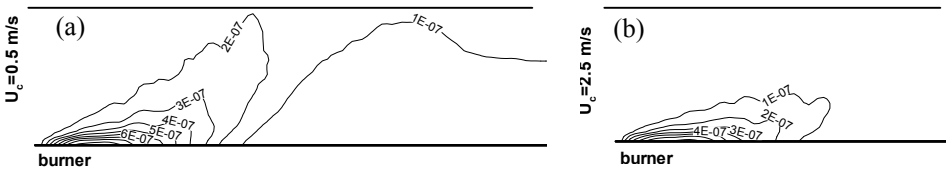


Fig. 9 - Predicted contours of soot volume fraction at $U_c$= 0.5 (a) and 2.5 m/s (b)

Comparison between predicted and measured mean flame-surface heat flux behind the pyrolysis zone, along the burning wall centerline (y=0.2 m) is presented in Figure 10. According to the experiment, for the high wind velocity ($U_c \geq 2$ m/s), the radiation flux is found to increase first from a low value near the pyrolysis zone to a maximum, and decrease later. For the low wind velocity ($U_c$<1.5 m/s), a monotonous decrease of the radiation flux is brought about.  As compared to the measured heat flux, the predicted one is relatively good for $U_c \leq 1.5$ m/s, and however, much higher in the fire section for

$U_c \geq 2$ m/s. The discrepancy between prediction and measurement may be due to the following factors :

- The maximum predicted temperature (Figure 7) is about 1400 °C near the burning surface, which seems too high for propane-air turbulent combustion due to the fast chemistry model.
- Another limitation is the radiation model for the intermediate scale fire simulation; also the maximum of the predicted soot volume fraction which is always close to the burning surface.
- Durning experiment, the heat feedback to the wall and radiation flux were measured by mounting the radiometers aperture of 150° view angle. A cooling water system was used to protect the wall material, yielding the measurement error with an uncertainty of 15-20%.

The other important source of information is the fraction of total flux by flame radiation, $\dot{q}_f/(\dot{q}_f + \dot{q}_c)$, to the solid surface, as shown in Figure 11. The measured convective flux seems to play a secondary role far away from the combusting portion of the fire for low wind velocity ($U_c \leq 1.5$ m/s). The fraction of total flux by radiation increases with decrease of the wind velocity, and the maximum contribution by radiation accounts for 80% of the total heat flux for $U_c$=0.7 m/s, and only 60% for $U_c$=2.5 m/s. However, in all the cases, the predicted contribution by radiation is higher than 70% of the total heat flux due to overprediction of the flame radiation flux.
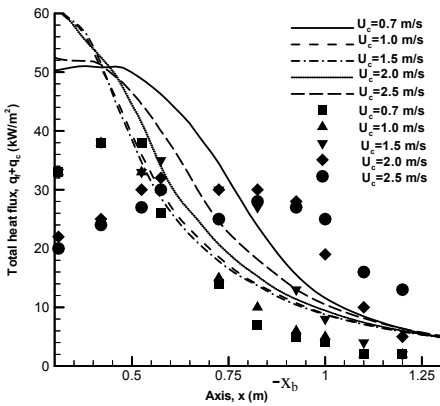


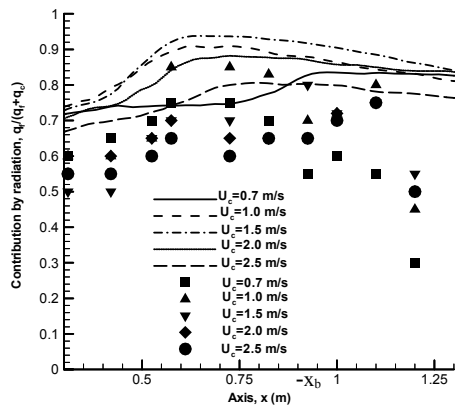Fig. 10 - Predicted (lines) and measured (symbols) heat flux as a function of the wind velocity

Fig. 11 - Predicted (lines) and measured (symbols) contribution by radiation as a function of the wind velocity

**CONCLUSION**

Large Eddy Simulation is tested by modeling wind-aided fire propagation behind a pyrolysis region along an intermediate scale model tunnel. Globally, the predicted mean flame shape by using EBU model is in relatively good agreement with experimental data. The behavior of the large-scale, highly transient intermittent flame and buoyant plume

inside the channel are reasonably well reproduced. The numerical results suggest that a weak wind-aided fire produces a complex time-dependent temperature and velocity fields due to buoyancy. It is found that for the low wind velocity ($U_c \leq 0.7$ m/s), the persistent flame is elongated near the burning surface, and however, the intermittent flame and buoyant smoke can be significantly tilted from the horizontal. Contribution by radiation is higher than 50% of the total heat flux for the low wind velocity, and convection can become a dominant mode of heat transfer for the high wind velocity ($U_c > 1.5$ m/s). The flame-surface heat flux is overpredicted as compared to measured one, particularly for high wind velocity, due to the overprediction of the temperature and soot formation near the fire section. Ongoing work is accounting for a Lagrangian dynamique subgrid-scale model of turbulence for the wind-aided fires. More research is also continuing about the turbulence effect on the soot formation to predict correctly flame radiation.

## REFERENCES

1.  Lavid, M. and Berlad, A.L., "Gravitational effects on Chemically Reacting Boundary Layer Flows over a Horizontal Flat Plate, " Sixteenth Symposium (International) on Combustion. Pittsburgh : The Combustion Institute, p.1157, 1976.
2.  Putnam, A.A., "A model study of wind-blown free-burning fires," Tenth Symposium (International) on Combustion. Pittsburgh : The Combustion Institute, p.1039, 1963.
3.  Apte, V.B., Bilger, R.W., Green, A.R. and Quintiere, J.G., "Wind aided turbulent flame spread and burning over large-scale horizontal PMMA surfaces," *Combustion and Flame*, 85:169, 1991.
4.  Wu, Y. and Bakar, M.Z.A., "Control of smoke flow in tunnel fires using longitudinal ventilation systems – a study of the critical velocity," *Fire Safety J*, 35:363-390, 2000.
5.  Kolb, G., "Etude d'une flamme non-prémélangée caractéristique d'un incendie en présence d'un écoulement forcé, " Ph.D. Thesis, Poitiers University, French.
6.  Kolb, G., Torero, J.L., Most, J.M. and Joulain, P., "Cross Flow Effects on the Flame Height of an Intermediate Scale Diffusion Flame, " Proceedings of the International Symposium on Fire and Technology, Seoul, Korea, pp.169-177, 1997.
7.  Woodburn, P. J. and Britter, R.E., "CFD Simulations of a Tunnel Fire-Part I-II, " *Fire Safety J*, 26:35-90, 1996.
8.  Fletcher, D.F., Kent, J.H., Apte, V.B. and Green, A.R., "Numerical Simulations of Smoke Movement from a Pool Fire in a Ventilated Tunnel, " *Fire Safety J*, 23:305-325, 1994.
9.  Mcgrattan, K.B, Glenn, P.F. and Jason, E.F., "Fire Dynamics Simulator – Technical Reference Guide, " NIST Technical Report, 2000.
10. Magnussen, F. and Hjertager, B.H., "On mathmatical modelling of turbulent combustion with special emphasis on soot formation and combustion," Sixteenth Symposium (International) on Combustion. Pittsburgh : The Combustion Institute, p.719, 1977.
11. Smagorinsky, J., "General circulation experiments with the primitive equations I. the basic experiment," Monthly Weather review, 91: 99, 1963.
12. Huggett, C., "Estimation of the rate of heat release by means of oxygen consumption measurements," *Fire and Materials*, 4 :61, 1980.
13. Modak, A.T., "Radiation from products of combustion, " *Fire Research*., 1, p.339, 1979.